Eur. Phys. J. B **8**, 555–568 (1999)

THE EUROPEAN PHYSICAL JOURNAL B

EDP Sciences

Dynamical mean-field study of the Mott transition in thin films

M. Potthoff[a] and W. Nolting

Institut für Physik, Humboldt-Universität zu Berlin, Invalidenstrasse 110, 10115 Berlin, Germany

Received 19 August 1998

Abstract. The correlation-driven transition from a paramagnetic metal to a paramagnetic Mott-Hubbard insulator is studied within the half-filled Hubbard model for a thin-film geometry. We consider simple-cubic films with different low-index surfaces and film thickness d ranging from $d = 1$ (two-dimensional) up to $d = 8$. Using the dynamical mean-field theory, the lattice (film) problem is self-consistently mapped onto a set of d single-impurity Anderson models which are indirectly coupled *via* the respective baths of conduction electrons. The impurity models are solved at zero temperature using the exact-diagonalization algorithm. We investigate the layer and thickness dependence of the electronic structure in the low-energy regime. Effects due to the finite film thickness are found to be the more pronounced the lower is the film-surface coordination number. For the comparatively open sc(111) geometry we find a strong layer dependence of the quasi-particle weight while it is much less pronounced for the sc(110) and the sc(100) film geometries. For a given geometry and thickness d there is a unique critical interaction strength $U_{c2}(d)$ at which all effective masses diverge and there is a unique strength $U_{c1}(d)$ where the insulating solution disappears. $U_{c2}(d)$ and $U_{c1}(d)$ gradually increase with increasing thickness eventually approaching their bulk values. A simple analytical argument explains the complete geometry and thickness dependence of U_{c2}. U_{c1} is found to scale linearly with U_{c2}.

PACS. 71.10.Fd Lattice fermion models (Hubbard model, etc.) – 71.30.+h Metal-insulator transitions and other electronic transitions – 73.50.-h Electronic transport phenomena in thin films

1 Introduction

Electron-correlation effects in systems with thin-film geometry have gained increasing interest in condensed-matter physics. In particular, there has been intense research on thermodynamic phase transitions to a symmetry-broken (*e.g.* magnetic) state below a critical temperature [1,2]. In magnetic thin films the thickness dependence of the order parameter, of the critical temperature as well as of the critical exponents has been investigated both, experimentally [3–6] and theoretically [7–10].

A thin film in three dimensions belongs to a two-dimensional universality class, regardless of the film thickness d [11]. Due to the Mermin-Wagner theorem [12], however, an effectively two-dimensional spin-isotropic system cannot display long-range magnetic order at any finite temperature. This is one important reason why anisotropies play a fundamental role for the understanding of thermodynamic phase transitions in thin films. The necessary inclusion of anisotropies, however, makes a theoretical description considerably more complicated.

For a quantum phase transition the situation is different: Symmetry breaking need not occur at the transition point, and the energy scale that is characteristic for the transition at zero temperature, remains meaningful at any finite temperature. Consequently, anisotropies are not vital for the understanding of a quantum phase transition in thin films: The transition can be studied within an isotropic model and at any temperature, starting from the monolayer ($d = 1$) up to the three-dimensional limit ($d \mapsto \infty$). From this point of view, following up the characteristics of a quantum phase transition as a function of d, may be the better defined and the simpler problem if compared with a thermodynamic transition.

One of the prime examples for a quantum phase transition is the correlation-driven transition from a paramagnetic metal to a paramagnetic insulator [13,14]. Generally, the Mott transition is of interest since strong electron correlations lead to low-energy electronic properties that cannot be understood within an independent-electron picture; the important correlation effects must be treated non-perturbatively. Conventional band theory is unable to provide a satisfactory description of the transition.

While magnetic phase transitions in thin films are traditionally studied within localized-moment models (Ising or Heisenberg model) [7–10], the possibly simplest generic model for the Mott transition is the Hubbard model [15]. Contrary to the localized-moment models, the Hubbard model describes itinerant electrons on a lattice which may form local moments as a consequence of the strong on-site Coulomb interaction. Starting from the early approaches

[a] e-mail: michael.potthoff@physik.hu-berlin.de

of Mott [13], Hubbard [16], and Brinkman and Rice [17], there has been extensive work on the Mott transition in the Hubbard model (for a recent overview see Ref. [14]). A thin-film geometry has not been considered up to now.

The following particular questions shall be addressed in the present study of the thin-film Mott transition: First, the breakdown of translational symmetry in the film normal direction introduces a layer dependence of physical quantities that characterize the transition. The layer dependence of the effective mass m^* or the double occupancy $\langle n_\uparrow n_\downarrow \rangle$, for example, is worth studying. Second, it has to be expected that there is a dependence on the film geometry. We can distinguish between surface effects and effects due to the finite film thickness: Surface effects are already present in thick films ($d \mapsto \infty$) and will be more pronounced for films with comparatively "open" surfaces, *i.e.* for surfaces where the nearest-neighbor coordination number is strongly reduced. For thin films there may be finite-thickness effects in addition. Here, the perturbation of the electronic structure introduced by one of the film surfaces affects the electronic structure in the vicinity of the other one; both surfaces can "interact" with each other. Third, it is not clear from the beginning whether or not there is a unique critical interaction strength U_c at which the whole film undergoes the transition. Analogously to magnetic transitions where an enhanced surface critical temperature is discussed [18–20], a modified U_c for the film surface might exist for thicker films. Finally, it is interesting to see the critical interaction strength U_c evolving as a function of d and to investigate how it approaches the bulk value. Again, the crossover from $D = 2$ to $D = 3$ dimensions should depend on the film geometry considered.

In the recent years, comprehensive investigations of the Mott transition have been performed [14,21] for the Hubbard model in infinite spatial dimensions [22,23]. The $D = \infty$ model is amenable to an exact solution by a self-consistent mapping onto an effective impurity problem which, however, must be treated numerically. Neglecting the spatial correlations, the same method can be applied for an approximate solution of the Hubbard model in any finite dimension $D < \infty$. This constitutes the so-called dynamical mean-field theory (DMFT) [23,21] which will be employed also for the present study. It is another intention of the paper to demonstrate that DMFT can successfully be applied to a film geometry.

The mean-field treatment of the Mott transition in $D < \infty$ rests on the assumption that spin- and charge fluctuations are reasonably local. In particular, the electronic self-energy is a local quantity within DMFT [24], $\Sigma_{ij}(E) = \delta_{ij}\Sigma_i(E)$. The relevance of non-local contributions for a qualitatively correct description of the Mott transition is not well understood at present. Effects of the non-locality of the self-energy can be estimated to some extent by conventional second-order U perturbation theory (SOPT). As is shown in reference [25], the local approximation is rather well justified for a $D = 3$ simple-cubic lattice. Non-local contributions become more important for $D = 2$ and especially for $D = 1$. With respect to the film geometry, the question is whether or not non-local contributions can be neglected also near the film surfaces. This has been investigated recently by means of SOPT applied to semi-infinite simple-cubic lattices [26]. The result is that at the surface the local approximation is as well justified as in the bulk.

There is an additional suppression of the effects of non-local fluctuations at half-filling: The low-energy electronic structure, being relevant for the transition, is governed by the (real) linear expansion coefficient $\beta_{ij} = d\Sigma_{ij}(E)/dE|_{E=0}$. Since $\mathrm{Re}\Sigma_{ij}(E)$ is a symmetric function of E in the particle-hole symmetric case and for nearest neighbors i and j, we have $\beta_{\langle ij \rangle} = 0$. Within SOPT the second nearest-neighbor term β_{ij} can be shown [26] to be smaller by about two orders of magnitude compared with the local one.

This shows that – at least for weak coupling – a local self-energy functional is a reliable approximation. Beyond the weak-coupling regime, however, the approximate locality actually is an assumption whose appropriateness has not yet been verified. We nevertheless expect DMFT to be a good starting point to study the Mott transition in a $D = 3$ film geometry.

We start our investigations by specifying the film geometries to be considered and discuss the DMFT approach with respect to thin films. In the first part of Section 3 we briefly focus on the Mott transition in the infinitely extended and translationally invariant model. After that the results for the films are analyzed in detail. Section 4 concludes the study.

2 DMFT for Hubbard films

We consider the Hubbard model at half-filling and zero temperature. Using standard notations, the Hamiltonian reads:

$$H = \sum_{\langle ij \rangle \sigma} t_{ij} c^\dagger_{i\sigma} c_{j\sigma} + \frac{U}{2} \sum_{i\sigma} n_{i\sigma} n_{i-\sigma}. \qquad (1)$$

The hopping integrals t_{ij} are taken to be non-zero between nearest neighbors i and j. $t \equiv -t_{\langle ij \rangle} = 1$ sets the energy scale. The thin-film geometry is realized by assuming i and j to run over the sites of a system that is built up from a finite number d of adjacent layers out of a three-dimensional periodic lattice. We study simple-cubic films with surface normals along the low-index [100], [110] and [111] directions. The model parameters are taken to be uniform, *i.e.* t and U are unchanged at the two film surfaces. With respect to the film normal, translational symmetry is broken; lateral translational symmetry, however, can be exploited by two-dimensional Fourier transformation: The hopping t_{ij} is transformed into a matrix $\epsilon_{\alpha\beta}(\mathbf{k})$ which is diagonal in the wave vector $\mathbf{k}$ of the first two-dimensional Brillouin zone (2DBZ). $\alpha, \beta = 1, ..., d$ label the different layers. For nearest-neighbor hopping and low-index sc films the Fourier-transformed hopping matrix is tridiagonal with respect to the layer indices. Its non-zero elements are given by: $\epsilon_\parallel(\mathbf{k}) \equiv \epsilon_{\alpha\alpha}(\mathbf{k})$ and $\epsilon_\perp(\mathbf{k}) \equiv \epsilon_{\alpha\alpha\pm1}(\mathbf{k})$. Let a

denote the lattice constant. For a sc(100) film the lateral and normal dispersions then read:

$$\epsilon_{\parallel}(\mathbf{k}) = 2t(\cos(k_x a) + \cos(k_y a)),$$
$$\epsilon_{\perp}(\mathbf{k})^2 = t^2. \tag{2}$$

Only the square of $\epsilon_{\perp}(\mathbf{k})$ will enter the physical quantities we are interested in. For the sc(110) geometry we have:

$$\epsilon_{\parallel}(\mathbf{k}) = 2t\cos(k_x a),$$
$$\epsilon_{\perp}(\mathbf{k})^2 = 2t^2 + 2t^2\cos(\sqrt{2}k_y a), \tag{3}$$

and the dispersions for the sc(111) films are:

$$\epsilon_{\parallel}(\mathbf{k}) = 0,$$
$$\epsilon_{\perp}(\mathbf{k})^2 = 3t^2 + 2t^2\cos(\sqrt{2}k_y a) + 4t^2\cos(\sqrt{3/2}k_x a)\cos(\sqrt{1/2}k_y a). \tag{4}$$

Note that the parallel dispersion vanishes since there are no nearest neighbors within the same layer. Due to the finite film thickness d, the local free ($U = 0$) density of states acquires a layer dependence: $\rho_i^{(0)}(E) = \rho_\alpha^{(0)}(E)$ for sites i within layer α. Particle-hole symmetry requires $\rho_\alpha^{(0)}(E)$ to be a symmetric function of the energy for each layer: On the bipartite lattice the odd moments $\int E^{2l+1}\rho_\alpha^{(0)}(E)dE$ ($l = 0, 1, ...$) vanish for all α (*cf.* Ref. [26]).

To study the transition from a paramagnetic metal at weak coupling to a paramagnetic Mott-Hubbard insulator at strong U, we restrict ourselves to the spin-symmetric and (laterally) homogeneous solutions of the mean-field equations. As usual [14] we thereby ignore antiferromagnetic ordering which is expected to be realized in the true ground state at any $U > 0$. The on-site Green function $G_{ii}(E) = \langle\langle c_{i\sigma}; c_{i\sigma}^\dagger\rangle\rangle_E$ thus depends on the layer index only: $G_{ii}(E) = G_\alpha(E)$. The same holds for the self-energy $\Sigma_{ii}(E) = \Sigma_\alpha(E)$ which is a local quantity within the mean-field approach. *Via* two-dimensional Fourier transformation we obtain from the Dyson equation:

$$G_\alpha(E) = \frac{1}{N_\parallel}\sum_{\mathbf{k}} R_{\alpha\alpha}^{-1}(\mathbf{k}, E)$$
$$R_{\alpha\beta}(\mathbf{k}, E) = (E+\mu)\delta_{\alpha\beta} - \epsilon_{\alpha\beta}(\mathbf{k}) - \delta_{\alpha\beta}\Sigma_\alpha(E), \tag{5}$$

where $N_\parallel$ is the number of sites within each layer ($N_\parallel \mapsto \infty$) and $\mathbf{k} \in$ 2DBZ. For the particle-hole symmetric case, the Fermi energy is given by $\mu = U/2$. Since $\epsilon_{\alpha\beta}(\mathbf{k})$ is tridiagonal, the matrix inversion is readily performed numerically by evaluating a continued fraction of finite depth which is given by the film thickness d (*cf.* Ref. [27]).

The layer-dependent self-energy $\Sigma_\alpha(E)$ shall be calculated within the dynamical mean-field theory (DMFT) [21,23]. This non-perturbative approach treats the local spin and charge fluctuations exactly. Neglecting spatial correlations, a *homogeneous* lattice problem can be mapped onto an effective impurity problem supplemented by a self-consistency condition [28,29]. For the present case of a thin Hubbard film we have to account for the non-equivalence of sites within different layers. Therefore, the film problem is mapped onto a set of d different impurity models with d self-consistency conditions.

The DMFT equations are solved by means of the following iterative procedure: We start with a guess for the self-energy $\Sigma_\alpha(E)$. This yields the on-site Green function $G_\alpha(E)$ *via* equation (5). In the next step we consider a single-impurity Anderson model (SIAM) [30] for each layer α:

$$H_{imp}^{(\alpha)} = \sum_\sigma \epsilon_d c_\sigma^\dagger c_\sigma + U n_\uparrow n_\downarrow + \sum_{\sigma,k=2}^{n_s} \epsilon_k^{(\alpha)} a_{k\sigma}^\dagger a_{k\sigma} + \sum_{\sigma,k=2}^{n_s}\left(V_k^{(\alpha)} a_{k\sigma}^\dagger c_\sigma + \text{H.c.}\right). \tag{6}$$

Here $\epsilon_k^{(\alpha)}$ and $V_k^{(\alpha)}$ denote the conduction-band energies and the hybridization strengths of the αth SIAM, respectively. It is sufficient to fix the free ($U = 0$) impurity Green function $G_\alpha^{(0)}(E)$ which is obtained from the αth DMFT self-consistency condition as:

$$G_\alpha^{(0)}(E) = \left(G_\alpha(E)^{-1} + \Sigma_\alpha(E)\right)^{-1}. \tag{7}$$

The crucial step is the solution of the impurity models for $\alpha = 1, ..., d$ to get the impurity self-energy $\Sigma_\alpha(E)$ which is required for the next cycle.

The computational effort needed for the solution of the impurity models scales linearly with the system size. It is enhanced by a factor $d/2$ compared with DMFT applied to the translationally invariant (bulk) Hubbard model if one takes into account the mirror symmetry with respect to the central layer of the film. Compared with the translationally invariant problem, we only found a slight increase in the number of cycles necessary for the convergence of the iterative procedure. The coupling between the different impurity problems *via* their respective baths of conduction electrons turns out to be weak.

The application of DMFT to the Hubbard model in thin-film geometry rests on exactly the same assumption that is necessary for the application of DMFT to any finite-dimensional system, namely on the local approximation for the self-energy. To be precise: the self-energy is taken to be local, $\Sigma_{ij}(E) = \delta_{ij}\Sigma_i(E)$, and to be given by the (diagrammatic) functional of the full *local* propagator $G_{ii}(E)$ only. This is sufficient to establish the mapping onto the impurity models and to derive the self-consistency condition. Since the local approximation is the only approximation used so far, the hopping between the layers is treated on the same level as the hopping within each layer. Near the film center and in the limit of infinite film thickness, our approach thus recovers the $D = 3$ (sc) bulk properties, *irrespective* of the particular film surface geometry. This represents a non-trivial check of the numerics.

For the solution of the SIAM we employ the exact-diagonalization (ED) method of Caffarel and Krauth [31].

The ED has proven its usefulness in a number of previous applications [21,31–34]. The main idea is to consider a SIAM with a *finite* number of sites n_s. This results in an obvious shortcoming of the method: ED is not able to yield a smooth density of states. Another disadvantage consists in the fact that finite-size effects are non-negligible whenever there is a small energy scale relevant for the problem to be investigated. With respect to the Mott transition, finite-size effects become important close to the critical interaction. On the other hand, there are a number of advantages: The ED method is based on a simple concept; it is easy to handle numerically and computationally fast if compared with the quantum Monte-Carlo (QMC) approach [29,35–38]. This is of crucial importance for a systematic study that covers a large parameter space. Opposed to QMC, the ED method is particularly well suited to study the model at $T = 0$.

Within the ED algorithm the functional equations for the self-energy are solved on a discrete mesh on the imaginary energy axis: $iE_n = i(2n+1)\pi/\widetilde{\beta}$ $(n = 0, 1, ..., n_{max})$. The *fictitious* inverse temperature $\widetilde{\beta}$ defines a low-energy cutoff, n_{max} represents a high-energy cutoff. Equation (7) provides the bath Green function $G^{(0)}_{\alpha}(iE_n)$ from which we have to fix the parameters of a SIAM with n_s sites. Following reference [31], this is achieved by minimization of the cost function

$$\chi^2 = \frac{1}{n_{max}+1} \sum_{n=0}^{n_{max}} \left| G^{(0)}_{\alpha}(iE_n)^{-1} - G^{(0)}_{\alpha,n_s}(iE_n)^{-1} \right| \quad (8)$$

with respect to the conduction-band energies $\epsilon^{(\alpha)}_k$ and the hybridization strengths $V^{(\alpha)}_k$ $(k = 2, ..., n_s)$. Thereby, $G^{(0)}_{\alpha}(iE_n)$ is approximated by the free $(U = 0)$ Green function of an n_s-site SIAM:

$$G^{(0)}_{\alpha,n_s}(iE_n - \mu)^{-1} = iE_n - \epsilon_d - \sum_{k=2}^{n_s} \frac{(V^{(\alpha)}_k)^2}{iE_n - \epsilon^{(\alpha)}_k} \cdot \quad (9)$$

Obviously, the method is exact for $n_s \mapsto \infty$ only. The convergence with respect to n_s, however, has been found to be exponentially fast [31]. Typically $n_s = 6 - 10$ sites are sufficient for interaction strengths not too close to the critical interaction. The results are independent of the low-energy cutoff provided that $\widetilde{\beta}^{-1}$ is chosen to be sufficiently small. Errors show up in the critical region close to the transition. Compared with the error due to the finite n_s, however, this is negligible. Once the SIAM is specified, Lanczòs technique [27] may be employed to calculate the ground state and the $T = 0$ impurity Green function $G_{\alpha}(iE_n)$. The local self-energy of the αth layer can be derived from the impurity Dyson equation $\Sigma_{\alpha}(iE_n) = G^{(0)}_{\alpha}(iE_n)^{-1} - G_{imp}(iE_n)^{-1}$.

3 Results and discussion

3.1 Bulk

Let us first concentrate on the $T = 0$ Mott transition in the translationally invariant Hubbard model before we come to the discussion of the results for the film geometry. This case has been the subject of numerous DMFT studies during the recent years [21,28,31,33,34,39–42]. Most investigations refer to the Bethe lattice with infinite connectivity where we have a semi-elliptical free density of states. However, within DMFT no qualitative changes are expected when considering the $D = 3$ simple-cubic lattice which also yields a symmetric and bounded free density of states. The $D = 3$ sc lattice is considered here since it represents the limit of infinite film thickness $d \mapsto \infty$ with respect to our film results.

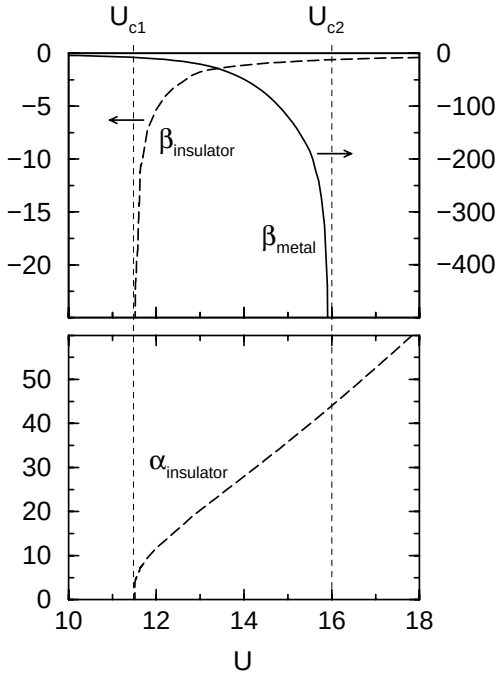

Fig. 1. Results for the (bulk) Mott transition in the half-filled Hubbard model as obtained within DMFT-ED. U dependence of the linear coefficient β in the low-energy expansion of $\Sigma(E)$ for the metallic (solid line) and the insulating solution (dashed line). The critical interactions U_{c1} and U_{c2} are indicated by the vertical lines. Lower panel: $1/E$ coefficient α in the low-energy expansion for the insulating solution. Calculation for a $D = 3$ simple-cubic lattice. Nearest-neighbor hopping $t = 1$. Width of free density of states: $W = 12$. $n_s = 8$.

Figure 1 shows the U dependence of the coefficients α and β in the low-energy Laurent expansion of the self-energy:

$$\Sigma(E) = \frac{\alpha}{E} + \frac{U}{2} + \beta E + \cdots \quad (10)$$

The calculation is performed for $n_s = 8$. For a metal, *i.e.* if $\alpha = 0$, the coefficient β yields the usual quasi-particle weight $z = (1 - \beta)^{-1}$ [43]. We find a metallic solution for interaction strengths up to a critical value $U_{c2} = 16.0$ ($U_{c2} = 4W/3$ in terms of the width of the free density of states $W = 12$). As U approaches U_{c2}, β diverges, *i.e.* the quasi-particle weight vanishes. At U_{c2} the metallic solution continuously coalesces with the insulating solution that is found for strong U. For decreasing U the insulating

phase ceases to exist below another critical interaction strength $U_{c1} = 11.5$ which is marked by the vanishing $1/E$ expansion coefficient α as well as by $\beta \mapsto -\infty$ (Fig. 1). We find $U_{c1} < U_{c2}$; there is a region where both, the metallic and the insulating solution, coexist [44].

A precise determination of the critical interactions, at least of U_{c2}, is not possible by means of the ED method (see next section). Qualitatively, however, the results are consistent with the findings for the $D = \infty$ Bethe lattice [28,31,33,34,39–42]: Within the iterative perturbation theory (IPT) [21,28] a narrow quasi-particle resonance is seen to develop at the Fermi energy for increasing U in the metallic solution. The spectrum has a three-peak structure, two additional charge-excitation peaks (Hubbard bands) show up at $E \approx \pm U/2$. For $U \mapsto U_{c2}$ the effective mass z^{-1} diverges as in the Brinkman-Rice variational approach [17]. On the other hand, at strong U the Hubbard bands are well separated by a gap in the insulating solution as in the Hubbard-III approach [16]. One can follow up the insulating solution by decreasing U down to $U = U_{c1}$. For $T = 0$ a coexistence of the solutions ($U_{c1} < U_{c2}$) has first been observed within IPT [39,40]. It is confirmed by ED [33] as well as by means of a recent numerical renormalization-group calculation (NRG) [42,45] which is particularly suited to study the critical regime. The comparison between the respective internal energies within IPT [21], ED [21,33] and NRG [45] as well as a simple argument mentioned in reference [41] show that the metallic phase is stable against the insulating one in the whole coexistence region up to U_{c2}: The $T = 0$ transition is found to be of second order.

One should also be aware of serious physical arguments [14,46] which have been raised against a transition scenario with two different critical interaction strengths. The exhaustion problem mentioned in reference [46] at least shows that a conclusive understanding of the Mott transition in $D = \infty$ has not yet been achieved. From the above discussion and our own results, however, we can conclude that the numerical evidences for the existence of a finite coexistence region are strong. Another problem is tackled in reference [47], where the concept of a preformed gap [21] is shown to be at variance with Fermi liquid theory. Our ED study cannot contribute to settle this interesting question since the detailed picture of the low-energy electronic structure in the limit $U \mapsto U_{c2}$ is concerned.

3.2 Films

In the following we discuss our results obtained by the ED approach to investigate the characteristics of the Mott transition in thin Hubbard films. Routinely, the calculations for the Hubbard films have been performed with $n_s = 8$ sites in the effective impurity problems. We systematically compared with $n_s = 6$ and also checked against $n_s = 10$ at a few data points. It turns out that there are no significant differences between the results for the different n_s as long as U is not too close to U_{c2} (see Fig. 10 and the related discussion). Choosing a small fictitious temperature $\widetilde{\beta}^{-1} = 0.0016\,W$ and a large high-energy cutoff

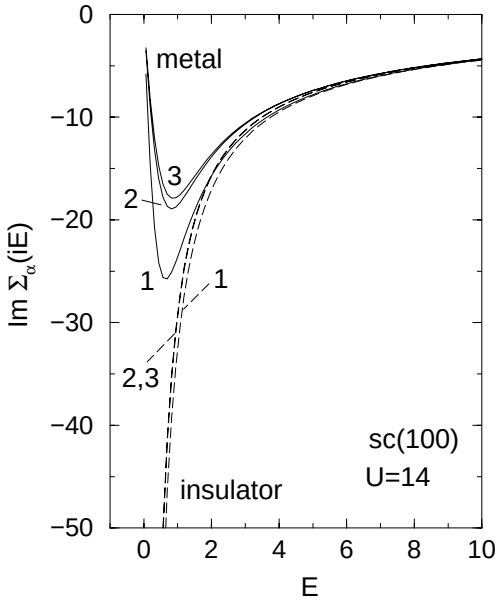

Fig. 2. Imaginary part of the layer-dependent self-energy Σ_α on the discrete mesh of the imaginary energies $iE_n = (2n + 1)\pi/\widetilde{\beta}$ ($\widetilde{\beta} = 50$, $\widetilde{\beta}^{-1} = 0.0016\,W$) for the $d = 5$ sc(100) film at $U = 14$. Results for the three inequivalent layers $\alpha = 1 - 3$ as indicated. $\alpha = 1$: surface layer. Solid lines: metallic phase. Dashed lines: metastable insulating phase.

$(2n_{max} - 1)\pi/\widetilde{\beta} > 2U$ ensures the results to be independent of the discrete energy mesh (see also discussion of Fig. 10). For the electron-hole symmetric case we can reduce the number of parameters in the multi-dimensional minimization (Eq. (8)) and for the DMFT self-consistency (Eq. (7)) by setting $\epsilon_k = -\epsilon_{k'}$ and $V_k^2 = V_{k'}^2$ for k, k' with $k + k' = n_s + 2$. For $n_s = 8$ and $d = 6$, which are typical values considered here, there are $(n_s - 1)d/2 = 21$ parameters to be determined. The stabilization of paramagnetic solutions has turned out to be unproblematic. A mixing of "old" and "new" parameters (50%), however, has been found to be necessary to obtain a converging self-consistency cycle for the sc(111) films. Apart from the coexistence of a metallic and an insulating solution in a certain U range, we always found a unique solution of the mean-field equations.

Figure 2 shows the imaginary part of the self-energy as obtained for a $d = 5$ sc(100) film. At $U = 14$ we find two solutions. In the metallic one there is a significant layer dependence of $\mathrm{Im}\,\Sigma_\alpha(iE)$ with a considerably larger slope $d\Sigma_\alpha/dE$ for $E \mapsto 0$ in the surface layer ($\alpha = 1$). This is plausible since the surface-layer sites have a reduced coordination number n resulting in a diminished variance $\Delta = nt^2$ of the free local density of states. Thus $U/\sqrt{\Delta}$ is larger compared with the film center tending to enhance correlation effects. The large values of $d\Sigma_\alpha/dE$ indicate that the system is close to the transition.

At $E = 0$ the imaginary part of the self-energy vanishes for all layers as it must be for a Fermi liquid (note that in Fig. 2 $\mathrm{Im}\,\Sigma$ is plotted on the discrete mesh iE_n only). A weak layer dependence is noticed for

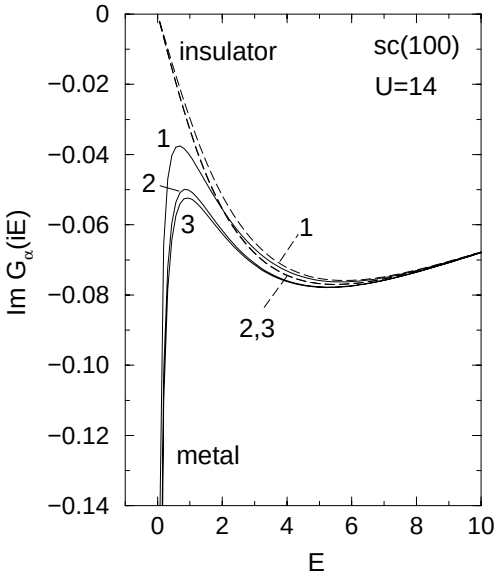

Fig. 3. The imaginary part of the Green functions corresponding to the self-energies in Figure 2.

the insulating solution. In this case $\mathrm{Im}\,\Sigma_\alpha(iE)$ diverges for $E \mapsto 0$.

The imaginary parts of the corresponding Green functions are shown in Figure 3. Again, the layer dependence is more pronounced for the metallic solution. For the insulating solution we have $\mathrm{Im}\,G_\alpha(i0^+) = 0$, *i.e.* a vanishing layer density of states at $E = 0$. Contrary, $\mathrm{Im}\,G_\alpha(i0^+)$ stays finite for the metal. The $E = 0$ value is given by equation (5) where

$$R_{\alpha\beta}(\mathbf{k}, i0^+) = (\mu + i0^+)\delta_{\alpha\beta} - \epsilon_{\alpha\beta}(\mathbf{k}) - \delta_{\alpha\beta}\Sigma_\alpha(0) = i0^+\delta_{\alpha\beta} - \epsilon_{\alpha\beta}(\mathbf{k}) = R_{\alpha\beta}(\mathbf{k}, i0^+)\Big|_{U=0}, \tag{11}$$

and where we used that $\mu = \Sigma_\alpha(0) = U/2$ for all layers α. This implies that (for a local Fermi liquid) the layer density of states at the Fermi energy $\rho_\alpha(0) = -\mathrm{Im}\,G_\alpha(i0^+)/\pi$ is unrenormalized by the interaction. As for $U = 0$, however, it is layer dependent. For the translationally invariant Hubbard model with local self-energy the pinning of the density of states is a well known and general consequence of Luttinger's sum rule [43]. In the case of Hubbard films (and within DMFT) there is a pinning of $\rho_\alpha(0)$ only for the case of half-filling since off half-filling $\Sigma_\alpha(0)$ acquires a layer dependence.

From the low-energy expansion of the self-energy for the metallic solution we can calculate the so-called layer-dependent quasi-particle weight

$$z_\alpha = \left(1 - \frac{d\Sigma_\alpha(E)}{dE}\Big|_{E=0}\right)^{-1}. \tag{12}$$

Once a self-consistent solution of the mean-field equations on the discrete energy mesh iE_n has been obtained, the self-energy can be determined in the entire complex energy plane, and there is no difficulty to calculate the derivative in equation (12). Let us briefly discuss the physical meaning of z_α which for a film geometry is slightly different compared with the bulk case [48]. Exploiting the lateral translational symmetry and performing a two-dimensional Fourier transformation, the Green function at low energies is given by:

$$G_{\alpha\beta}(\mathbf{k}, E) \equiv \frac{1}{N_\parallel}\sum_{i_\parallel j_\parallel} e^{i\mathbf{k}(\mathbf{R}_{i_\parallel} - \mathbf{R}_{j_\parallel})}\langle\langle c_{i_\parallel\alpha\sigma}; c^\dagger_{j_\parallel\beta\sigma}\rangle\rangle = \sqrt{z_\alpha}\left(\frac{\mathbf{1}}{\mathbf{E1} - \mathbf{T}(\mathbf{k})}\right)_{\alpha\beta}\sqrt{z_\beta}. \tag{13}$$

Here $(\mathbf{T}(\mathbf{k}))_{\alpha\beta} = \sqrt{z_\alpha}\epsilon_{\alpha\beta}(\mathbf{k})\sqrt{z_\beta}$ is the renormalized hopping matrix. $i_\parallel$ and $j_\parallel$ label the $N_\parallel$ sites in the layers α and β, respectively, and $\mathbf{k} \in$ 2DBZ. Only the linear term in the expansion of the self-energy is taken into account. For each wave vector $\mathbf{k}$ the matrix $\mathbf{T}(\mathbf{k})$ can be diagonalized by a unitary transformation which is mediated by a matrix $U_{\alpha r}(\mathbf{k})$. The d eigenvalues $\eta_r(\mathbf{k})$ of $\mathbf{T}(\mathbf{k})$ ($r = 1, ..., d$) yield the dispersions of the quasi-particle bands near the Fermi energy and determine the d one-dimensional Fermi "surfaces" in the 2DBZ *via* $\eta_r(\mathbf{k}) = 0$. As can be seen from equation (13), when $\mathbf{k}$ approaches the rth Fermi surface there is a discontinuous drop of the αth momentum-distribution function

$$n_\alpha(\mathbf{k}) = -\frac{1}{\pi}\int_{-\infty}^{0}\mathrm{Im}\,G_{\alpha\alpha}(\mathbf{k}, E + i0^+)\,dE, \tag{14}$$

which is given by:

$$\delta n_\alpha(\mathbf{k}^r_{\mathrm{F}}) = \left|U_{\alpha r}(\mathbf{k}^r_{\mathrm{F}})\right|^2 \cdot z_\alpha. \tag{15}$$

Summing over the d Fermi surfaces, we have:

$$z_\alpha = \sum_{r=1}^{d}\delta n_\alpha(\mathbf{k}^r_{\mathrm{F}}). \tag{16}$$

The momentum-distribution function can be calculated on the imaginary energy axis *via*:

$$n_\alpha(\mathbf{k}) = \frac{1}{2} + \lim_{\beta\mapsto\infty}\frac{2}{\beta}\,\mathrm{Re}\sum_{n=0}^{\infty}G_{\alpha\alpha}(\mathbf{k}, iE_n). \tag{17}$$

Figure 4 shows $n_\alpha(\mathbf{k})$ along a high-symmetry direction in the 2DBZ for the $d = 5$ sc(100) film. For the non-interacting system the 5 bands $\eta_r(\mathbf{k})$ are occupied at the $\overline{\Gamma} = (0, 0)$ point and empty at $\overline{M} = (\pi, \pi)$. Consequently, all bands cross the Fermi energy along the $\overline{\Gamma M}$ direction, and discontinuinities can be seen at 5 Fermi wave vectors $\mathbf{k}^r_{\mathrm{F}}$. Due to symmetries $U_{\alpha r}(\mathbf{k}^r_{\mathrm{F}})$ may vanish in some cases. For example, at the Fermi wave vector $\mathbf{k}_{\mathrm{F}} = (\pi/2, \pi/2)$ we have $\epsilon_\parallel(\mathbf{k}_{\mathrm{F}}) = 0$, and one can easily prove $(1, 0, -1, 0, 1)$ to be an eigenvector of the hopping matrix $\epsilon_{\alpha\beta}(\mathbf{k}_{\mathrm{F}})$ with eigenvalue $\eta = 0$. This implies that there is no discontinuity of $n_{\alpha=2}$ (and $n_{\alpha=4}$) at $\mathbf{k} = (\pi/2, \pi/2)$.

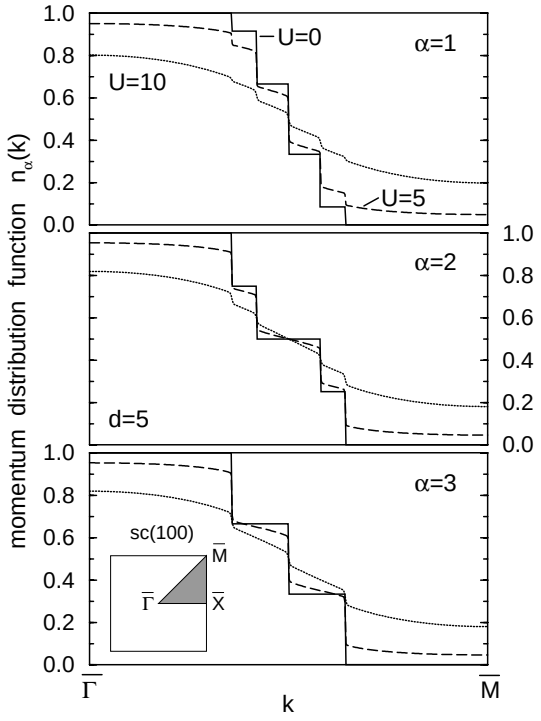

Fig. 4. Momentum distribution function $n_\alpha(\mathbf{k})$ for the (non-equivalent) layers $\alpha = 1, 2, 3$ along a high-symmetry direction in the irreducible part of the 2DBZ. Results for the $d = 5$ sc(100) film at different U.

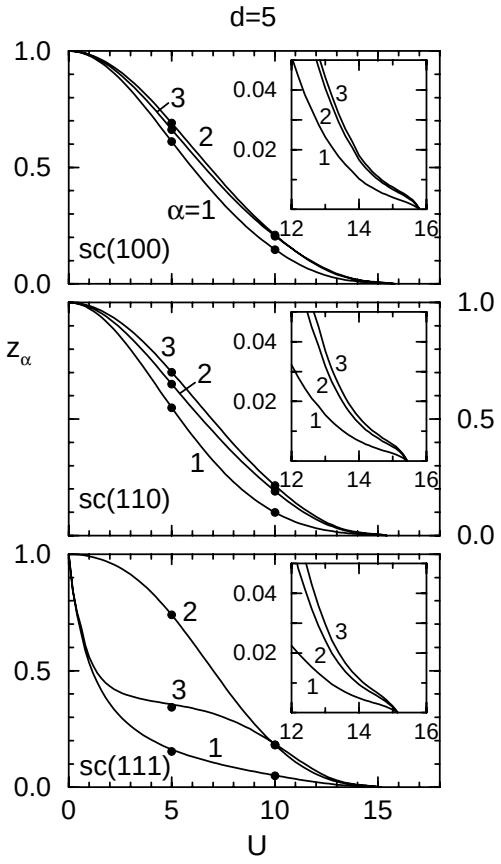

Fig. 5. Layer-dependent quasi-particle weight z_α as a function of U for a $d = 5$ layer film in sc(100), sc(110) and sc(111) geometry. Calculation for $n_s = 8$ (solid lines) and $n_s = 10$ (dots). The insets show $z_\alpha(U)$ in the critical regime.

For the interacting system, $\delta n_\alpha(\mathbf{k}^r_{\mathrm{F}})$ is reduced by the layer-dependent factor $z_\alpha < 1$. The Fermi surfaces themselves, however, remain unchanged since $\det(\epsilon_{\alpha\beta}(\mathbf{k})) = 0$ implies $\det(\sqrt{z_\alpha}\epsilon_{\alpha\beta}(\mathbf{k})\sqrt{z_\beta}) = 0$ for any $\mathbf{k}$. Generally speaking, the invariance of the Fermi surfaces is a consequence of the manifest particle-hole symmetry at half-filling and of the local approximation for the self-energy.

From equation (13) we have:

$$z_\alpha = \frac{1}{N_\parallel}\sum_{\mathbf{k}}\int_{-\infty}^{\infty} -\frac{1}{\pi}\mathrm{Im}\, G^{(\mathrm{coh})}_{\alpha\alpha}(\mathbf{k}, E + i0^+)\, dE, \quad (18)$$

which shows that z_α also yields the weight of the coherent quasi-particle peak in the layer-resolved density of states. z_α can serve as an "order parameter" for the Mott transition. For $z_\alpha = 0$ the system is a Mott-Hubbard insulator.

Figure 5 shows z_α as a function of U in the metallic solution for the sc(100), sc(110) and the sc(111) films with thickness $d = 5$. The layer-dependent quasi-particle weight decreases from its non-interacting value $z_\alpha = 1$ to $z_\alpha = 0$. In the weak-coupling regime there is a quadratic dependence $1 - z_\alpha(U) \propto U^2$ which is consistent with perturbation theory in U [26]. An almost linear dependence is seen for the sc(111) film for $\alpha = 1$ and $\alpha = 3$ which indicates an early breakdown of perturbation theory in this case. For each film geometry considered, there is a unique critical interaction U_{c2} where all functions $z_\alpha(U)$ simultaneously approach zero; the whole system can be either metallic or insulating.

Depending on the film geometry, we notice a weak (sc(100)) or a rather strong (sc(111)) layer dependence of the quasi-particle weight. For weak and intermediate couplings we may observe an oscillatory dependence on α (sc(100)). For U closer to U_{c2}, the behavior changes qualitatively; here z_α monotonously increases with increasing distance from a film surface. This is a typical effect which is also observed for still thicker films. Figure 6 illustrates this fact. It shows a film profile of the quasi-particle weight for a $d = 17$ sc(100) film at $U = 6$ (z_α oscillating) and $U = 12$ (z_α monotonous).

In all cases the quasi-particle weight of the surface layer $z_{\alpha=1}$ is significantly reduced compared with $\alpha = 2, 3$. As has been mentioned above, this can be attributed to the lowered film-surface coordination number. For $d = 5$ (Fig. 5) the critical interaction U_{c2} is significantly reduced compared with the bulk ($d \mapsto \infty$) value. For the sc(100) film we find $U_{c2} = 15.8$, for the sc(110) $U_{c2} = 15.4$, and for the sc(111) geometry we have $U_{c2} = 15.2$. This has to be compared with the bulk value $U_{c2} = 16.0$ (see Fig. 1). The critical interaction is the lower the more open is the film surface. We have $n_{(100)} = 5$, $n_{(110)} = 4$, $n_{(111)} = 3$ for the coordination numbers at the film surfaces while in

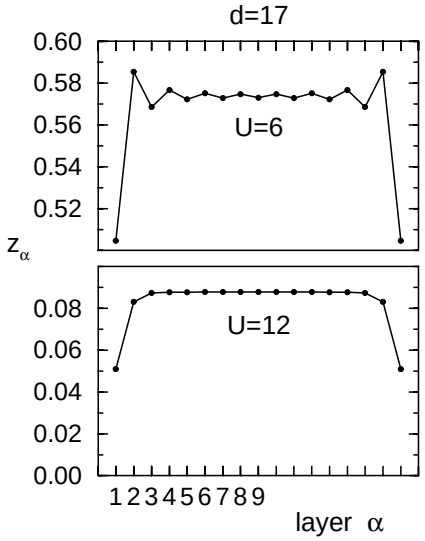

Fig. 6. Layer dependence of the quasi-particle weight for $U = 6$ and $U = 12$ in the $d = 17$ sc(100) film.

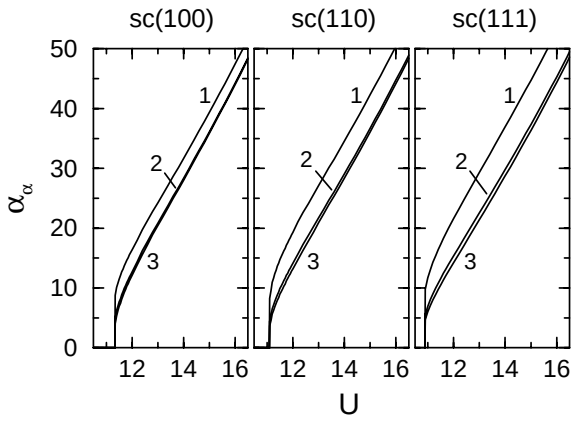

Fig. 7. Layer-dependent $1/E$ (low-energy) coefficient as a function of U for the insulating phase and different film geometries. Film thickness: $d = 5$.

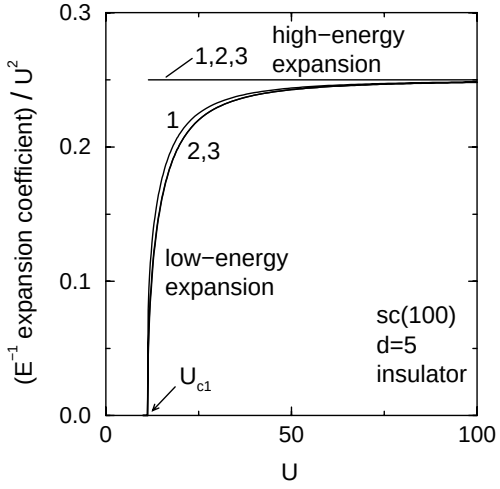

Fig. 8. Layer-dependent $1/E$ coefficient in the low- and the high-energy expansion of the self-energy as a function of U. Insulator on the $d = 5$ sc(100) film.

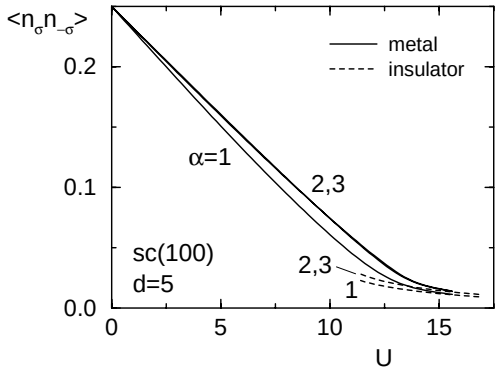

Fig. 9. Layer-dependent double occupancy $\langle n_{i\sigma} n_{i-\sigma} \rangle$ (with $i \in \alpha$) as a function of U. Metallic (solid lines) and the insulating solution (dashed lines) for the $d = 5$ sc(100) film.

the film center $n = 6$. (Errors for the U_{c2} values are discussed below, the observed trends are not affected.)

The same trend is also found for the critical interaction U_{c1} where the insulating solution disappears. Figure 7 shows the U dependence of the $1/E$ coefficient in the low-energy expansion of the self-energy. For the sc(100) film we find $U_{c1} = 11.3$ while $U_{c1} = 11.1$ for the sc(110) geometry. With $U_{c1} = 10.9$ the lowest value is observed for the sc(111) film. Contrary to the quasi-particle weight in the metallic solution, there is always a monotonous increase of the $1/E$ coefficient when passing from the film center to one of the surfaces for the insulating solution. In particular, the surface-layer value is significantly enhanced. As $U \mapsto U_{c1}$, the $1/E$ coefficient non-continuously drops to zero. For the thin-film geometries this is much more apparent than for the bulk (see Fig. 1).

The almost linear U dependence of the $1/E$ coefficient well above U_{c1} (Fig. 7) alters for still higher U: The regime of very strong Coulomb interaction is shown in Figure 8 for the sc(100) film. Eventually, for $U \mapsto \infty$, there is a quadratic dependence of the $1/E$ coefficient on U. It smoothly approaches the quadratic U dependence of the high-energy expansion of the self-energy: $\Sigma_\alpha(E) = U/2 + U^2/4E + \cdots$ [49]. The system behaves more and more atomic-like.

The layer-dependent average double occupancy is shown in Figure 9 as a function of U. For small U and all layers, $\langle n_\uparrow n_\downarrow \rangle$ decreases linearly as in the Brinkman-Rice solution [17]. At $U = U_{c2}$ it smoothly joins with the (non-zero) average double occupancy of the insulating solution. For the insulator $\langle n_\uparrow n_\downarrow \rangle$ increases with decreasing U down to U_{c1}. For both, the metal and the insulator, double occupancies are suppressed more strongly at the film surfaces compared with the film center. Again, this is due to the stronger effective Coulomb interaction $U/\sqrt{\Delta}$ which results from the reduced variance Δ of the surface free local density of states.

Within the ED method a second-order transition from the metallic to the insulating phase is predicted at

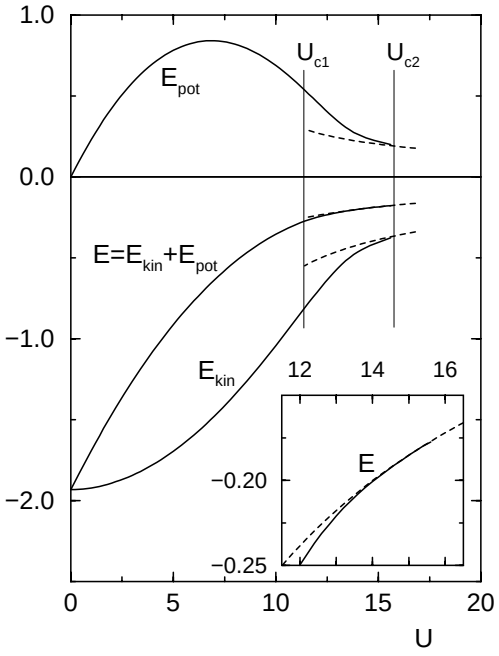

Fig. 10. Kinetic, potential and total energy per site as functions of U in the metallic (solid lines) and the insulating solution (dashed lines) for the $d = 5$ sc(100) film.

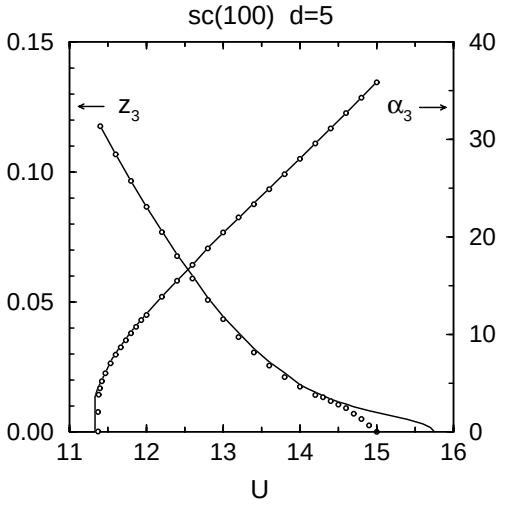

Fig. 11. U dependence of the quasi-particle weight z_3 and of the coefficient α_3 in the central layer of the $d = 5$ sc(100) film. Solid lines: $n_s = 8$ (metal) and $n_s = 7$ (insulator). Circles: $n_s = 10$ (metal) and $n_s = 9$ (insulator).

$U = U_{c2}$. This can be seen from the U dependence of the respective internal energies: A layer-dependent kinetic and potential energy per site can be defined as:

$$T_\alpha = \sum_{j\sigma} t_{ij} \langle c^\dagger_{i\sigma} c_{j\sigma} \rangle \qquad (i \in \alpha)$$
$$V_\alpha = U \langle n_{i\uparrow} n_{i\downarrow} \rangle \qquad (i \in \alpha). \tag{19}$$

The double occupancy $\langle n_{i\uparrow} n_{i\downarrow} \rangle$ and thus the potential energy can be obtained from the (ED) solution of the impurity models directly. The kinetic energy may be calculated from:

$$T_\alpha = \lim_{\beta \mapsto \infty} \frac{4}{\beta} \mathrm{Re} \sum_{n=0}^{\infty} (iE_n G(iE_n) - 1) + \frac{U}{2} - 2U \langle n_{i\uparrow} n_{i\downarrow} \rangle. \tag{20}$$

Figure 10 shows the kinetic ($E_{kin} = (1/d) \sum_\alpha T_\alpha$), potential ($E_{pot} = (1/d) \sum_\alpha V_\alpha$) and total energy per site ($E = E_{kin} + E_{pot}$) for the $d = 5$ sc(100) film. Due to the presence of the film surface, the absolute value of the kinetic energy per site at $U = 0$ is somewhat lowered compared with kinetic energy per site of the $D = 3$ lattice which amounts to $E^{(D=3)}_{kin} = -2.005$. Comparing the different energies in the coexistence region $U_{c1} < U < U_{c2}$, we notice that the gain in kinetic energy is almost perfectly outweighted by the loss in potential energy when passing from the insulating to the metallic solution at a given U. A similar cancellation effect has been observed beforehand for the $D = \infty$ Bethe lattice [33]. Figure 10 shows a remaining very small difference in the total energy which favors the metallic solution in the entire coexistence region.

Although this is a consistent result within the ED method, it must be considered with some care: For the metallic solution close to U_{c2} the relevant energy scale is determined by the width of the quasi-particle resonance near $E = 0$. This width is approximately given by $z_\alpha W$ where W is the free band width. Since $z_\alpha \mapsto 0$ for $U \mapsto U_{c2}$, one should expect that finite-size effects become important here and that an accurate determination of the internal energy cannot be achieved by the ED method. The same holds for the determination of U_{c2} (and also of critical exponents). With the ED method we cannot access the very critical regime.

Figure 11 gives an example. Here we compare the quasi-particle weight z_3 at the center of the $d = 5$ sc(100) film obtained for $n_s = 8$ with the result for $n_s = 10$. We notice that finite-size effects are unimportant for $z_s > 0.01$. Generally, $n_s = 8$ sites are sufficient for convergence if U is well below U_{c2}. This can also be seen in Figure 5 where a comparison with the results for $n_s = 10$ is shown at a few points. For $z < 0.01$, however, there are non-negligible differences: U_{c2} is lowered by about 5% when passing from $n_s = 8$ to $n_s = 10$ (Fig. 11). This gives an estimate for the error in the determination of U_{c2}. The smallest reliable value for the quasi-particle weight z_{min} determines the "energy resolution" ΔE that can be achieved by the ED method for a given n_s. We have $\Delta E \approx z_{min} W$. For $n_s = 8$ and with $z_{min} \approx 0.01$ this yields $\Delta E \approx 0.1$. The error that is introduced by the finite low-energy cutoff is of minor importance compared with the error due to finite-size effects. This is plausible since the smallest fictitious Matsubara frequency can be made as small as ΔE (here we have $\pi \widetilde{\beta}^{-1} \approx 0.05$).

In the particle-hole symmetric case there is always one conduction-band energy with $\epsilon^{(\alpha)}_k = 0$ (per layer). The corresponding hybridization strength $V^{(\alpha)}_k$ vanishes as $U \mapsto U_{c2}$ in the self-consistent calculation. Therefore,

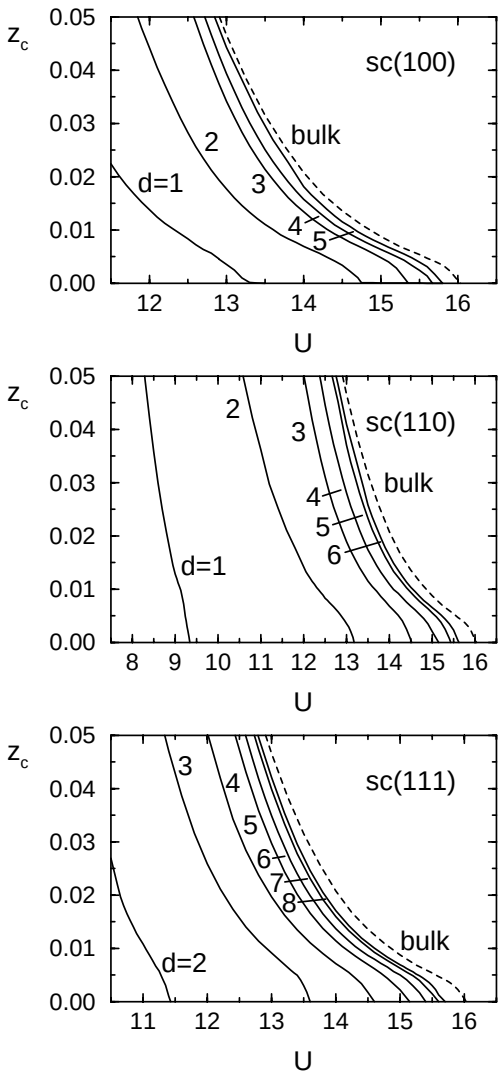

Fig. 12. Quasi-particle weight of the central layer $\alpha = d/2$ ($\alpha = (d+1)/2$, respectively) as a function of U for sc(100), sc(110) and sc(111) films (solid lines) with a thickness d ranging from $d = 1$ (two-dimensional Hubbard model) up to $d = 5$ ($d = 6$, $d = 8$, respectively) and the result for $d \mapsto \infty$ (bulk, dashed line). Note the different U scales.

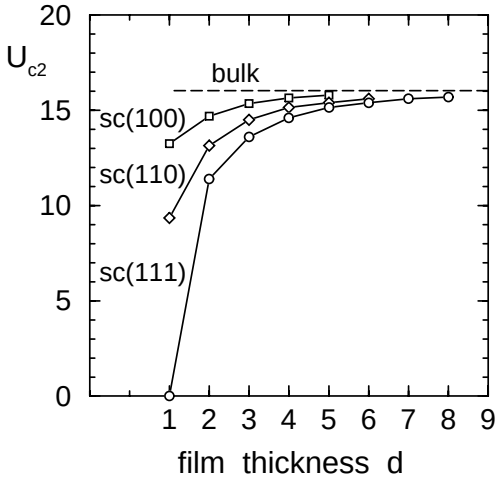

Fig. 13. Thickness dependence of the critical interaction U_{c2} for sc(100), sc(110) and sc(111) films.

for the insulator at $U > U_{c2}$ we are effectively left with $n_s - 1$ sites that are coupled *via* the hybridization term. The metallic solution for $n_s = 8$ ($n_s = 10$) thus merges with the insulating solution for $n_s = 7$ ($n_s = 9$) at U_{c2}. Since the quasi-particle resonance is absent in the insulating solution, there are no problems with the n_s convergence in this case. The comparison between the results for $n_s = 7$ and $n_s = 9$ is also shown in Figure 11. The critical interaction U_{c1} can be determined much more precisely.

A basic question in a study of the Mott transition in thin films concerns the thickness dependence of the critical interactions U_{c2} and U_{c1}. Since it is the general trend that is of primary interest, the mentioned ambiguity in the determination of U_{c2} plays a minor role only. For all geometries and thicknesses considered, we found U_{c2} and U_{c1} to be unique, *i.e.* for a given system all layer-dependent quasi-particle weights and also all $1/E$ coefficients vanish at a common critical value of the interaction, respectively. It is thus sufficient to concentrate on the quantities at the film center.

Figure 12 shows the central-layer quasi-particle weight z_c as a function of U for the different systems in the region close to $U_{c2}(d)$. It is worth mentioning that for all three film geometries and for all $d \geq 2$ the functions $z_c(U)$ are more or less only shifted rigidly to lower interactions compared with the result $z(U)$ for the bulk (which of course is independent from the choice of the film surface). This is in clear contrast to the trend of $z_c(U)$ for weaker interactions (see the result for the sc(111) film in Fig. 5, for example): In the critical regime but also at weaker interactions where finite-size effects are unimportant, the U dependence of z_α is rather insensitive to details of the film geometry. On the other hand, the shift of $z_c(U)$ with respect to $z(U)$ does depend on the thickness d. In all cases $z_c(U)$ shifts to higher interaction strengths with increasing d and converges to the bulk curve $z(U)$ finally. This also implies that without any exception z_c increases with increasing d at a given U. We can state that the general trends are remarkably simple.

From the zero of $z_c(U)$ we can determine the critical interaction U_{c2} for a given geometry and thickness. The results for the different systems are summarized in Figure 13. U_{c2} is a monotonously increasing function of d for the sc(100), the sc(110) as well as for the sc(111) films. For a finite thickness, $U_{c2}(d)$ is always smaller than the bulk value which is apparently approached only in the limit $d \mapsto \infty$. For a given film thickness, U_{c2} increases when passing from the sc(111) to the sc(110) and to the sc(100) film. (Note that for the $d = 1$ sc(111) film $U_{c2} = 0$ since there is no intra-layer hopping in this case.) The convergence with respect to d is the fastest for the sc(100) and the slowest for the sc(111) films. These trends seem to be related to the differences in the film-surface coordination numbers: $n_{(100)} = 5$, $n_{(110)} = 4$, $n_{(111)} = 3$.

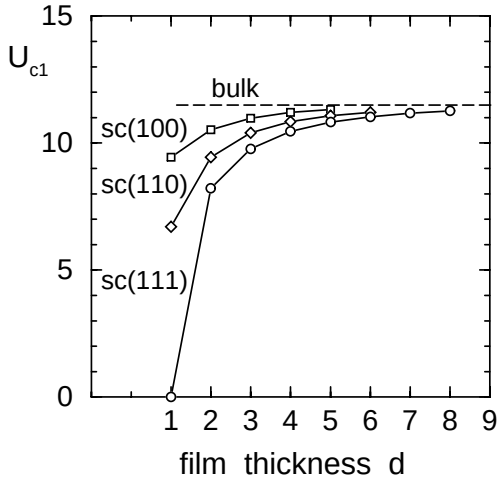

Fig. 14. Thickness dependence of U_{c1}.

The interaction strength at which the central-layer $1/E$ coefficient α_c drops to zero determines U_{c1} (see Fig. 7). Its thickness dependence is shown in Figure 14 for the different geometries. The result is rather surprising: Apart from small uncertainties in the determination of U_{c2} and U_{c1}, the relative thickness and geometry dependence of U_{c1} is the same as that of U_{c2}. Only the absolute values for U_{c1} are smaller: $U_{c1}(d)$ converges to the bulk value $U_{c1} = 11.5$ which is well below $U_{c2} = 16.0$. If we rescale $U_{c1}(d)$ for the different geometries by the same (bulk) factor $r = U_{c2}/U_{c1} \approx 1.39$, we end up with the results for $U_{c2}(d)$ shown in Figure 13 within a tolerance ($|r \cdot U_{c1}(d) - U_{c2}(d)|/U_{c2} < 0.005$) that is much smaller than *e.g.* the error in the determination of U_{c2} due to finite-size effects. The latter is irrelevant here if one assumes U_{c2} to be overestimated by the same constant factor, for the bulk and for the films, which would only change the ratio r. Looking at the trends in the results for $n_s = 8$ in Figure 12, this assumption is quite plausible. The found relation between U_{c2} and U_{c1} is surprising because the disappearance of the insulating solution for $U \mapsto U_{c1}$ is expected to be of different nature compared with the breakdown of the Fermi-liquid metallic phase as $U \mapsto U_{c2}$.

For U_{c2}, all the details of its geometry and thickness dependence can be understood by a simple but instructive argument. The main idea has first been developed by Bulla [50] for the $D = \infty$ case. Here we discuss a generalization for the film geometries:

The argument assumes that for $U \mapsto U_{c2}$ one can disregard the effects of the high-energy charge excitation peaks at $E \approx \pm U/2$ and that the quasi-particle resonance near $E = 0$ results from a SIAM hybridization function $\Delta^{(\alpha)}(E) = \sum_k (V_k^{(\alpha)})^2/(E + \mu - \epsilon_k^{(\alpha)})$ that consists of a single pole at $E = 0$:

$$\Delta^{(\alpha)}(E) \mapsto \frac{\Delta_N^{(\alpha)}}{E} \cdot \tag{21}$$

With the index N we refer to the Nth step in the iterative solution of the DMFT self-consistency equation. For each layer $\alpha = 1, ..., d$ the one-pole structure of $\Delta^{(\alpha)}(E)$ corresponds to an $n_s = 2$ site SIAM with a conduction-band energy at $\epsilon^{(\alpha)} = U/2$ and hybridization strength $V^{(\alpha)} = (\Delta_N^{(\alpha)})^{1/2}$. The analytic solution up to second order in $V^{(\alpha)}/U$ (*cf.* Ref. [51]) yields two peaks in the impurity spectral function at $E \approx \pm U/2$ as well as two peaks near $E = 0$ which build up the Kondo resonance for $U \mapsto U_{c2}$. The weight of the resonance is thus given by:

$$z_\alpha = 2 \cdot \frac{18 (V^{(\alpha)})^2}{U^2} = \frac{36}{U^2} \Delta_N^{(\alpha)}. \tag{22}$$

In the self-consistent solution this is also the layer-dependent quasi-particle weight which determines the coherent part of the film Green function in the low-energy regime *via* equation (13). The coherent part of the on-site Green function in the αth layer may be written as:

$$G_\alpha^{(\mathrm{coh.})}(E) = z_\alpha \cdot \widetilde{G}_\alpha(E) = \frac{z_\alpha}{E - \widetilde{M}_\alpha^{(2)} F_\alpha(E)} \cdot \tag{23}$$

Here, $\widetilde{G}_\alpha(E)$ is the on-site element of the free film Green function, but calculated for the renormalized hopping matrix $\epsilon_{\alpha\beta}(\mathbf{k}) \mapsto \sqrt{z_\alpha}\, \epsilon_{\alpha\beta}(\mathbf{k}) \sqrt{z_\beta}$ (see Eq. (13)). The second expression represents the first step in a continued-fraction expansion which involves the second moment $\widetilde{M}_\alpha^{(2)} = \int dE\, E^2\, \widetilde{G}_\alpha(E)$ of $\widetilde{G}_\alpha(E)$. For the remainder we have $F_\alpha(E) = 1/E + \mathcal{O}(E^{-2})$.

Starting from equation (21) in the Nth step, the DMFT self-consistency equation (7) yields a new hybridization function *via* $\Delta^{(\alpha)}(E) = E - (\epsilon_d - \mu) - \Sigma_\alpha(E) - G_\alpha(E)^{-1}$. Using $\epsilon_d = 0$, $\mu = U/2$, $\Sigma_\alpha(E) = U/2 + (1 - z_\alpha^{-1})E + \cdots$ and equation (23), we get:

$$\Delta^{(\alpha)}(E) = \frac{1}{z_\alpha} \widetilde{M}_\alpha^{(2)} F_\alpha(E) \tag{24}$$

for energies close to $E = 0$. Insisting on the one-pole structure of $\Delta^{(\alpha)}(E) \stackrel{!}{=} \Delta_{N+1}^{(\alpha)}/E$ for $U \mapsto U_{c2}$, we must have $F_\alpha(E) = 1/E$. This amounts to replacing the coherent part of the film Green function by the simplest Green function with the same moments up to the second one. To express $\Delta_{N+1}^{(\alpha)}$ in terms of $\Delta_N^{(\alpha)}$, we still need $\widetilde{M}_\alpha^{(2)}$. Let us introduce the intra- and inter-layer coordination numbers q and p (*e.g.* $q = 4$ and $p = 1$ for the sc(100) geometry). The second moment is easily calculated by evaluating an (anti-)commutator of the form $\langle [\, [[c, \widetilde{H}_0]_-, \widetilde{H}_0]_-, c^\dagger]_+ \rangle$. This yields:

$$\widetilde{M}_\alpha^{(2)} = z_\alpha (q z_\alpha + p z_{\alpha-1} + p z_{\alpha+1})\, t^2. \tag{25}$$

We also define the following tridiagonal matrix with dimension d:

$$\mathbf{K}(U) = \frac{36\, t^2}{U^2} \begin{pmatrix} p & q & & \\ p & q & p & \\ & p & q & .. \\ & & .. & .. \end{pmatrix} \cdot \tag{26}$$

Inserting (25) and (22) into (24), yields a "linearized" self-consistency equation for $U \mapsto U_{c2}$:

$$\Delta_{N+1}^{(\alpha)} = \sum_{\beta} K_{\alpha\beta}(U)\Delta_N^{(\beta)}. \tag{27}$$

A fixed point of $\mathbf{K}(U)$ corresponds to a self-consistent solution. Let $\lambda_r(U)$ denote the eigenvalues of $\mathbf{K}(U)$. We can distinguish between two cases: If $|\lambda_r(U)| < 1$ for all $r = 1, ..., d$, there is the trivial solution $\lim_{N\mapsto\infty} \Delta_N^{(\alpha)} = 0$ only. This situation corresponds to the insulating solution for $U > U_{c2}$. Contrary, if there is at least one $\lambda_r(U) > 1$, $\Delta_N^{(\alpha)}$ diverges exponentially as $N \mapsto \infty$. This indicates the breakdown of the one-pole model for the hybridization function in the metallic solution for $U < U_{c2}$. The critical interaction is thus determined by the maximum eigenvalue:

$$\lambda_{max}(U_{c2}) = 1. \tag{28}$$

The eigenvalues of a tridiagonal matrix (26) can be calculated analytically for arbitrary matrix dimension d [52]: The $\lambda_r(U)$ are the zeros of the dth degree Chebyshev polynomial of the second kind. Solving (28) for U_{c2} then yields:

$$U_{c2}(d, q, p) = 6t\sqrt{q + 2p\cos\left(\frac{\pi}{d+1}\right)}. \tag{29}$$

Figure 15 shows that the numerical results for U_{c2} can be well described by this simple formula. Plotting U_{c2}^2 against $q+2p\cos(\pi/(d+1))$, yields a linear dependence as a good approximation. The slope in the linear fit to the data, however, turns out to be $(6.61t)^2 > (6t)^2$. This shows that there is a *systematic* overestimation of the critical interaction by about 10% compared with equation (29). Partially, this has to be ascribed to finite-size effects in the ED method since the error estimated from the results in Figure 11 is of the same order of magnitude. (As mentioned before, the fact that the error is a systematic one, is explained by the very simple trends seen in Fig. 12.) On the other hand, we also have to bear in mind that (29) rests on some simplifying assumptions.

While we have achieved a satisfactory understanding of the results for U_{c2}, it remains unclear to us why equation (29) (with the factor $6t$ replaced by a suitable constant) also well describes the thickness and geometry dependence of U_{c1}. Again, Figure 15 shows a linear trend. The slope is $(4.74t)^2$. The above-developed argument, however, obviously breaks down.

It is instructive to compare these results with the analogous results for a thermodynamic phase transition in thin films. Within the mean-field approach, the layer-dependent magnetization m_α in Ising films with coupling constant J is determined by the self-consistency equation:

$$m_\alpha = \tanh\left(\frac{J}{2k_BT}(qm_\alpha + pm_{\alpha+1} + pm_{\alpha-1})\right). \tag{30}$$

The equation can be linearized for temperatures T near the Curie temperature T_C where $m_\alpha \ll 1$. Comparing with equation (27) yields the following analogies:

$$m_\alpha \Leftrightarrow z_\alpha, \quad J/2 \Leftrightarrow 36t^2, \quad k_BT \Leftrightarrow U^2, \quad k_BT_C \Leftrightarrow U_{c2}^2. \tag{31}$$

The exact Curie temperature in thick ($d \mapsto \infty$) Ising films is expected [53,54] to obey the power law $(T_c(\infty) - T_c(d))/T_c(\infty) = C_0 d^{-\lambda}$ where the shift exponent $\lambda = 1/\nu$ is related to the ($D = 3$) critical exponent ν of the correlation function. Within the mean-field approach to the magnetic phase transition in Ising films one obtains $\lambda = 2$.

The same exponent is found within dynamical mean-field theory applied to the Mott transition in Hubbard films. Expanding equation (29) in powers of $1/d$, we obtain:

$$\frac{U_{c2} - U_{c2}(d, q, p)}{U_{c2}} = C_0(q, p) \cdot d^{-\lambda}, \tag{32}$$

where U_{c2} denotes the bulk value, $C_0(q, p) = \pi^2 q/(q + 2p)$ and $\lambda = 2$ the exponent.

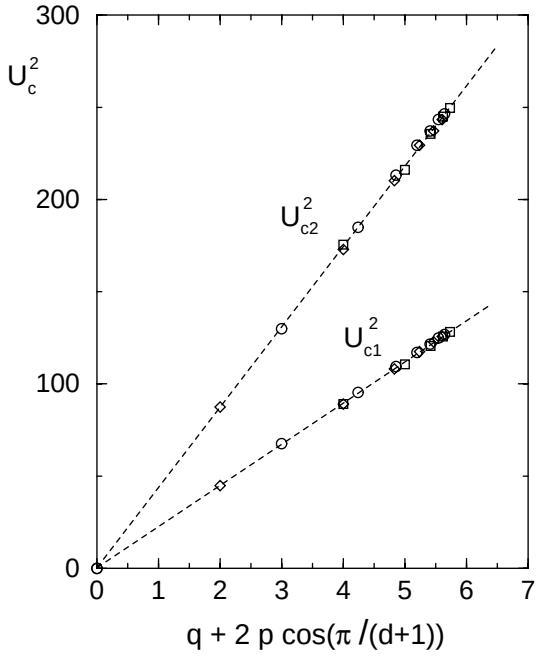

Fig. 15. Critical interactions U_{c2}^2 and U_{c1}^2 for sc(100) (squares), sc(110) (diamonds) and sc(111) films (circles) as in Figures 13 and 14, but plotted against $q + 2p\cos(\pi/(d + 1))$. The dashed lines are linear fits to the data.

4 Conclusion

By the invention of dynamical mean-field theory we are in a position to treat itinerant-electron models on the same footing as does the Weiss molecular-field theory with respect to localized spin models. To gain a first insight into collective magnetism for thin-film and surface geometries, the molecular-field approach has successfully been applied to the Ising or the Heisenberg model in the past. It is

well-known that the reduced system symmetry may result in characteristic modifications of the magnetic properties which are interesting on their own but also with respect to technical applications. The Weiss theory is able to describe a major number of magnetic properties qualitatively correct.

To study the correlation-induced Mott transition from a paramagnetic metal to a paramagnetic insulator, we need to consider an itinerant-electron model. Presumably, the Hubbard model is the simplest one in this respect. Just as the Weiss theory for the magnetic properties of Ising and Heisenberg films, the DMFT provides the first step in an understanding of the Mott transition and the related electronic properties in Hubbard films. This has been the central idea of the present study. We have generalized the mean-field equations for the application to systems with reduced translational symmetry and have solved them using the exact-diagonalization method. Let us briefly list up the main results found:

Similar to the results for the infinite-dimensional Bethe lattice, we find a metallic and an insulating solution of the mean-field equations at $T = 0$ for all film geometries considered. These coexist in a certain range of the interaction strength. The metallic solution is stable against the insulating one in the whole coexistence region (however, in the critical regime the ED approach is questionable).

Generally, the breakdown of translational symmetry with respect to the film normal direction leads to modifications of the electronic structure. For film thickness $d \mapsto \infty$ these disappear in the bulk, while surface effects are still present. The finite film thickness as well as the presence of the surface manifest themselves in a significant layer dependence of the on-site Green function and the self-energy for both, the metallic and the insulating solution. The layer dependence is found to be the more pronounced the more open is the film surface. In thicker films surface effects quickly diminish when passing from the top layer to the film center.

In particular, we have considered the so-called layer-dependent quasi-particle weight z_α for the metallic phase as a function of U, d and geometry. For $U \neq 0$, $z_\alpha < 1$ is the reduction factor of the discontinuous drop of the momentum-distribution function in the αth layer at each of the d one-dimensional Fermi-"surfaces" or, equivalently, the weight of the coherent quasi-particle peak in the local density of states of the αth layer. In all cases the quasi-particle weight at the film surfaces is found to be significantly reduced which is due to the surface enhancement of the effective Coulomb interaction $U/\sqrt{\Delta}$ (Δ is the variance of the free local density of states). At the film surfaces the electrons are "heavier", double occupancies are suppressed more effectively. The layer dependence of the quasi-particle weight is oscillatory in some cases at small and intermediate interaction strengths. As U approaches the critical regime, the behavior changes qualitatively; here z_α is always monotonously increasing with increasing distance from a film surface. Furthermore, for fixed U, z_α always increases with increasing d – the general trends are remarkably simple.

The low-energy electronic structure in the insulating solution is governed by the $1/E$ coefficient in the low-energy expansion of the self-energy. Generally, the layer dependence of the coefficient is less spectacular compared with the layer dependence of z_α in the metallic solution. At the film surfaces the $1/E$ coefficient is somewhat enhanced and in all cases monotonously decreases with increasing distance from a surface.

For a given film geometry and thickness there is a unique critical interaction U_{c2} at which all (layer-dependent) effective masses z_α^{-1} diverge. This implies that the whole film is either metallic or a Mott insulator. For all cases investigated, we did not find a surface phase that differs from the bulk phase. This may change if non-uniform model parameters, *e.g.* a modified surface U, are considered. The question is left for future investigations.

While a precise determination of the critical interaction is not possible by means of the ED approach, general trends can be derived safely. It is found that U_{c2} is strongly geometry and thickness dependent. It monotonously increases with increasing film thickness and smoothly approaches the bulk value from below. For finite d, U_{c2} is the smaller and the convergence to the bulk value is the slower the more open is the film surface. The same trends are also seen for the critical interaction U_{c1} at which the insulating solution disappears. In fact, within numerical accuracy a simple relation, $U_{c2}(d) = r \cdot U_{c1}(d)$, seems to hold. The geometry and thickness dependence of U_{c2} can be understood qualitatively by (approximately) linearizing the mean-field equations for $U \mapsto U_{c2}$. After proper rescaling, the resulting analytical expression for $U_{c2}(d, q, p)$ can even quantitatively reproduce the numerical data. The argument, however, is not applicable to the critical interaction U_{c1} and thus cannot explain the "empirically" found relation between U_{c1} and U_{c2}. An effective, linearized theory that is valid for $U \mapsto U_{c1}$ remains to be constructed. Calculating the Curie temperature of Ising films within the molecular-field theory, yields exactly the same trends. This analogy suggests that the observed geometry and thickness dependence may be *typical* for the mean-field treatment of the problem. Whether or not there are qualitative changes if $U_{c1,2}(d, q, p)$ could be calculated beyond mean-field theory, remains to be another open problem.

Finally, one could think of an experimental investigation of the Mott transition in thin films. The present study shows that the strong thickness dependence of the critical interaction has its origin in the reduced coordination number at the film surface. A monotonous increase of the critical interaction with increasing d should thus be expected also for temperatures above the Néel temperature where we have a magnetically disordered state. Studying the Mott transition in a bulk material, one needs to "vary U" (or temperature) experimentally. Contrary, for a thin-film geometry the transition may take place also by varying d. If it is possible to grow crystalline films of a metallic material which in the bulk is close to the Mott transition, one may observe insulating behavior in ultrathin films and a transition to a metallic phase with increasing thickness.

The authors would like to thank R. Bulla (MPI für Physik komplexer Systeme, Dresden) for helpful discussions and for drawing our attention to reference [50] prior to publication. This work is supported by the Deutsche Forschungsgemeinschaft within the SFB 290.

References

1. R. Allenspach, J. Magn. Mat. **129**, 160 (1994).
2. K. Baberschke, Appl. Phys. A **62**, 417 (1996).
3. W. Dürr, M. Taborelli, O. Paul, R. Germar, W. Gudat, D. Pescia, M. Landolt, Phys. Rev. Lett. **62**, 206 (1989).
4. C.M. Schneider, P. Bressler, P. Schuster, J. Kirschner, J.J. de Miguel, R. Miranda, Phys. Rev. Lett. **64**, 1059 (1990).
5. Yi Li, K. Baberschke, Phys. Rev. Lett. **68**, 1208 (1992).
6. M. Farle, K. Baberschke, U. Stetter, A. Aspelmeier, F. Gerhardter, Phys. Rev. B **47**, 11571 (1993).
7. Qiang Hong, Phys. Rev. B **41**, 9621 (1990).
8. R.P. Erickson, D.L. Mills, Phys. Rev. B **43**, 11527 (1991).
9. P.J. Jensen, H. Dreyssé, K.H. Bennemann, Surf. Sci. **269/270**, 627 (1992).
10. P. Schilbe, S. Siebentritt, K.-H. Rieder, Phys. Lett. A **216**, 20 (1996).
11. M.E. Fisher, J. Vac. Sci. Technol. **10**, 665 (1973).
12. N.D. Mermin, H. Wagner, Phys. Rev. Lett. **17**, 1133 (1966).
13. N.F. Mott, Philos. Mag. **6**, 287 (1961).
14. F. Gebhard, *The Mott Metal-Insulator Transition* (Springer, Berlin, 1997).
15. M.C. Gutzwiller, Phys. Rev. Lett. **10**, 159 (1963); J. Hubbard, Proc. R. Soc. London, A **276**, 238 (1963); J. Kanamori, Prog. Theor. Phys. (Kyoto) **30**, 275 (1963).
16. J. Hubbard, Proc. R. Soc. London, A **281**, 401 (1964).
17. W.F. Brinkman, T.M. Rice, Phys. Rev. B **2**, 4302 (1970).
18. D.L. Mills, Phys. Rev. B **3**, 3887 (1971).
19. J.L. Morán-López, J.M. Sanchez, Phys. Rev. B **39**, 9746 (1989).
20. M. Potthoff, W. Nolting, Phys. Rev. B **55**, 2741 (1997).
21. A. Georges, G. Kotliar, W. Krauth, M.J. Rozenberg, Rev. Mod. Phys. **68**, 13 (1996).
22. W. Metzner, D. Vollhardt, Phys. Rev. Lett. **62**, 324 (1989).
23. D. Vollhardt, in *Correlated Electron Systems*, edited by V.J. Emery (World Scientific, Singapore, 1993), p. 57.
24. E. Müller-Hartmann, Z. Phys. B **74**, 507 (1989).
25. H. Schweitzer, G. Czycholl, Z. Phys. B **83**, 93 (1991).
26. M. Potthoff, W. Nolting, Z. Phys. B **104**, 265 (1997).
27. R. Haydock, in *Solid State Physics, Advances in Research and Applications*, edited by H. Ehrenreich, F. Seitz, D. Turnbull (Academic, London, 1980), Vol. 35.
28. A. Georges, G. Kotliar, Phys. Rev. B **45**, 6479 (1992).
29. M. Jarrell, Phys. Rev. Lett. **69**, 168 (1992).
30. P.W. Anderson, Phys. Rev. **124**, 41 (1961).
31. M. Caffarel, W. Krauth, Phys. Rev. Lett. **72**, 1545 (1994).
32. Qimiao Si, M.J. Rozenberg, G. Kotliar, A.E. Ruckenstein, Phys. Rev. Lett. **72**, 2761 (1994).
33. M. Rozenberg, G. Moeller, G. Kotliar, Mod. Phys. Lett. B **8**, 535 (1994).
34. L. Laloux, A. Georges, W. Krauth, Phys. Rev. B **50**, 3092 (1994).
35. J.E. Hirsch, R.M. Fye, Phys. Rev. Lett. **56**, 2521 (1986).
36. M.J. Rozenberg, X.Y. Zhang, G. Kotliar, Phys. Rev. Lett. **69**, 1236 (1992).
37. A. Georges, W. Krauth, Phys. Rev. Lett. **69**, 1240 (1992).
38. M. Jarrell, T. Pruschke, Z. Phys. B **90**, 187 (1993).
39. A. Georges, W. Krauth, Phys. Rev. B **48**, 7167 (1993).
40. M.J. Rozenberg, G. Kotliar, X.Y. Zhang, Phys. Rev. B **49**, 10181 (1994).
41. G. Moeller, Qimiao Si, G. Kotliar, M. Rozenberg, D.S. Fisher, Phys. Rev. Lett. **74**, 2082 (1995).
42. R. Bulla, A.C. Hewson, T. Pruschke, J. Phys.-Cond. Matter **10**, 8365 (1998).
43. E. Müller-Hartmann, Z. Phys. B **76**, 211 (1989).
44. In their original work [31], Caffarel and Krauth did not find a significant coexistence of a metallic and an insulating solution. Using the same ED algorithm, this was corrected later by Rozenberg *et al.* in reference [33] who found coexisting solutions at interaction strengths well below U_{c2}. It was also shown that both ED methods, the one of reference [31] ("star geometry") and that of reference [32] ("two-chain geometry"), yield almost equal results and a consistent picture of the transition (see also [21]).
45. R. Bulla, private communication.
46. D.E. Logan, Ph. Nozières, Phil. Trans. R. Soc. London A **356**, 249 (1998).
47. S. Kehrein, Phys. Rev. Lett. **81**, 3912 (1998).
48. J.M. Luttinger, Phys. Rev. **119**, 1153 (1960).
49. M. Potthoff, T. Herrmann, W. Nolting, Euro. Phys. J. B **4**, 485 (1998).
50. R. Bulla, (unpublished).
51. A.C. Hewson, *The Kondo Problem to Heavy Fermions* (Cambridge University Press, Cambridge, 1993).
52. W.-H. Steeb, *Problems in Theoretical Physics*, (BI Wissenschaftsverlag, Mannheim, 1990), Vol. 1.
53. M.E. Fisher, A.E. Ferdinand, Phys. Rev. Lett. **19**, 169 (1967).
54. G.A.T. Allan, Phys. Rev. B **1**, 352 (1970).